



City Research Online

City, University of London Institutional Repository

Citation: Qian, K., Lan, D., Zhang, L., Fu, F. & Fang, Q. (2022). Robustness of Post-Tensioned Concrete Beam-Column Sub-assemblies under Various Column Removal Scenarios. *Journal of Structural Engineering*, 148(5), doi: 10.1061/(ASCE)ST.1943-541X.0003324

This is the accepted version of the paper.

This version of the publication may differ from the final published version.

Permanent repository link: <https://openaccess.city.ac.uk/id/eprint/27334/>

Link to published version: [https://doi.org/10.1061/\(ASCE\)ST.1943-541X.0003324](https://doi.org/10.1061/(ASCE)ST.1943-541X.0003324)

Copyright: City Research Online aims to make research outputs of City, University of London available to a wider audience. Copyright and Moral Rights remain with the author(s) and/or copyright holders. URLs from City Research Online may be freely distributed and linked to.

Reuse: Copies of full items can be used for personal research or study, educational, or not-for-profit purposes without prior permission or charge. Provided that the authors, title and full bibliographic details are credited, a hyperlink and/or URL is given for the original metadata page and the content is not changed in any way.

Robustness of Post-Tensioned Concrete Beam-Column Sub-assemblies under Various Column Removal Scenarios

Kai Qian¹ M. ASCE, Dong-Qiu Lan², Lu Zhang³ M. ASCE, Feng Fu⁴ F. ASCE, Qin Fang⁵

ABSTRACT

To fully recognize the load-resisting mechanisms of posttensioned concrete (PC) structures with realistic boundary conditions against disproportionate collapse, four beam-column sub-assemblies were extracted from a prototype building; and the side columns and joints are reproduced to reflect the actual boundary condition. The parametric analysis was conducted, including location of the removed column (middle or penultimate) and strand profile (straight or parabolic). In addition, two reinforced concrete (RC) counterparts were tested as control group. Test results indicate that the unbonded post-tensioning strand (UPS) was able to enhance the structural robustness by increasing compressive arch action capacity of RC beams and developing catenary action. Compared with RC specimens, both PC specimens achieved much higher load resistance; herein, the PC specimen with straight strand profile obtained the highest load resistance due to two strands used, while the PC specimen with parabolic profile had higher deformation capacity. However, the existence of UPS increased the tensile force demand to the side column, leading to the flexural tension failure of the side column when the loss of a penultimate column was considered. Finally, analytical study was carried out to quantify the load resistance from each dominant load resisting mechanisms.

Author Keywords: Post-tensioned Concrete; Boundary Condition; Strand Profile; Disproportionate collapse

¹Professor, Guangxi Key Laboratory of New Energy and Building Energy Saving at Guilin University of Technology, Guilin, China, 541004, (corresponding author), Email: qiankai@glut.edu.cn

²Graduate Student, College of Civil Engineering and Architecture at Guangxi University, Nanning, China 530004, Email: landongqiu@st.gxu.edu.cn

³Professor, Guangxi Key Laboratory of New Energy and Building Energy Saving at Guilin University of Technology, Guilin, China, 541004, Email: zhanglu@glut.edu.cn

⁴Senior Lecturer in Structural Engineering, School of Mathematics, Computer Science and Engineering, City, University of London, U.K., Email: Feng.Fu.1@city.ac.uk

⁵Professor, Army Engineering University, Nanjing, China, 210007. Email: fangqinjs@139.com

INTRODUCTION

Disproportionate collapse is defined as the final collapse of a building is disproportionate to the initial local damage due to the development of local damage in a domino manner (Ellingwood 2006). Catastrophes occasionally occurred in the past decades, such as the recently collapse of a 12-story residential building in Miami on June 24, 2021. It is realized that the partial loss of load resistance in the ground column due to foundation settlement or reinforcement corrosion is the possible causes. Partial or entire loss of the load resistance of the column can also be caused by many other threats such as vehicle impact, terrorist attack, gas explosion, extreme environment, construction mistake, and so on.

In the existing design guidelines for disproportionate collapse (GSA 2013, DoD 2016), both threat-dependent and non-threat dependent design approaches are proposed. The former required to predict the possible abnormal load, which may bring difficulties in practical design. The latter, as known as alternate load path (ALP) approach, assumes hypothetical local damage by the removal of one or several critical vertical load bearing members, but ignores all other potential damage to adjacent structural elements, the non-threat specific nature allows researchers to perform experimental program conveniently.

Based on the ALP approach, extensive studies have been carried out to understand the load-resisting mechanisms of RC structures (Sasani et al.2007, Yi et al. 2008, Orton et al. 2009, Su 2009, Sheffield et al. 2011, FarhangVesali et al. 2013, Yu and Tan 2013 a, Yu and Tan 2013b, Pham and Tan 2014, Yu et al. 2014, Xiao et al. 2015, Qian et al. 2017, Peng et al. 2018, Ma et al. 2020;

Deng et al. 2020, Yu et al. 2020, Zhou et al. 2021) and precast concrete structures (Nimse et al. 2014, Qian and Li 2019, Zhou et al. 2019, Qian et al. 2021). The Vierendeel action was found to be a viable load-resisting mechanism to resist disproportionate collapse from a test on an actual 10-story RC building (Sasani et al. 2007). Compressive arch action (CAA) and tensile catenary action (TCA) developed in beams were also investigated extensively (FarhangVesali et al. 2013, Yu and Tan 2013 b, Deng et al. 2020, Qian et al. 2021). Conversely, the membrane actions developed in RC slabs were relatively insufficient (Pham and Tan 2014, Lu et al. 2017, Yu et al. 2020). The mobilization of CAA and TCA corresponds to compressive and tensile axial force developed in RC beams (Yu and Tan 2013a, Yu and Tan 2013b, Su et al. 2009, Vali pour et al. 2015, Deng et al. 2020).

Currently, few studies on prestressed concrete structures were reported in literature (Keyvani and Sasani 2015, Keyvani and Sasani 2016, Qian et al. 2018, Qian et al. 2019, Tian et al. 2020, Qian et al. 2021, Husain et al. 2021). And also, most of those studies use unbonded posttensioned strands (UPS). They concluded that the UPS was able to enhance structural robustness effectively, while the enhancement was mainly attribute to increased total area of reinforcement regardless of the prestressing magnitude (Husain 2021). The parametric study on profile of the strand shown that straight and parabolic profiles resulted in similar structural resistance but different failure modes (Husain 2021, Qian et al. 2021). Those studies helped the practitioners to understand load-resisting mechanisms of precast concrete structures; but all of them didn't reproduce the actual boundary condition because the boundary of specimens in those tests were simplified by enlarged column to provide sufficient boundary stiffness. The conclusions drawn by studies based on different boundary conditions could be inconsistent.

To fill this gap, six specimens consist of four posttensioned concrete (PC) specimens and two RC counterparts were tested to understand the structural behavior of PC frames subjected to

various column removal scenarios. Other than the previous tested beam-column sub-assemblies, in this paper, the side columns and joints were reproduced to reflect the boundary condition more realistic.

Experimental Programme

Specimen Detailing

To explore the behavior of posttensioned concrete (PC) frames under the column removal scenarios, four PC beam-column sub-assemblies with different strands profiles and boundary conditions were fabricated. The prototype building is a large commercial PC moment-resisting frame, which was designed according to ACI 318-14 (2014). The dead load and live load are taken as 5.5 kPa and 2.0 kPa, respectively. The PC specimens with different strand profiles are designed to have same level of bending moment capacity. The specimens were 1/2 scaled from the prototype frame due to the limitation of Lab. facility capacity. The main details between prototype and scaled models are compared in Table 1. The design variables include the position of column removal (middle or penultimate) and strand profile (straight or parabolic). To quantify the effects of the strands, two additional RC specimens with identical dimension and reinforcement details as the PC specimens were constructed for reference. The detailed characteristics of the specimens are tabulated in Table 2. The naming criterion follows: Specimen PCM-S indicates a PC specimen subjected to Middle column removal, while the strand profile is Straight. Similarly, Specimen PCP-P indicates a PC specimen under a Penultimate column removal, while the strand profile is Parabolic.

Fig. 1 shows the design details of specimens under a middle column removal scenario, the specimens include one removed column stub, two side columns, two beams, and two overhanging beams. The clear beam span is 2750 mm. The beam and column cross-section is $250 \times 150 \text{ mm}^2$

and $250 \times 250 \text{ mm}^2$, respectively. The beam was reinforced by 2T12 at the bottom and 3T12 at the top, while the curtailment of reinforcement was considered in the design. The transverse reinforcement of R6 with a spacing of 50 mm and R6 with a spacing of 100 mm was installed in the reinforced zone and non-reinforced zone, respectively. T12 and R6 represent deformed rebars with diameters of 12 mm and round rebar with diameter of 6 mm, respectively. Two UPS with 7-wire and nominal diameter of 12.7 mm were installed in parallel with the axis of beam of PCM-S, whereas only one UPS with parabolic profile was installed in PCM-P. The UPS was designed with effective prestress of $0.65 f_{pu}$, where f_{pu} is nominal ultimate strength of the UPS of 1860 MPa. It should be noticed that the RC details of the corresponding specimens subjected to penultimate column removal were identical to those subjected to middle column removal except without the overhanging beam on the right side.

Material Properties

Based on the compressive concrete test, average cylinder compressive strengths of RCM and RCP were 39 MPa while for PCM-S, PCM-P, PCP-S, and PCP-P were 36 MPa. The properties of reinforcement and strand are listed in Table 3.

Instrumentation Layout and Test Setup

Fig.2a shows the experimental setup. Figs. 2b and c show the instrumentations layouts. The pin support and horizontal restraints on the top of side columns were applied to simulate contra-flexural points of the side column. As illustrated in Fig. 2, the top of the side columns and the overhanging beams were connected to an A-frame by horizontal rollers. The concentrated load was applied by a hydraulic jack (Item 1 in Fig. 2a). As only planar beam-column sub-assemblies were constructed, to prevent out-of-plane failure, a steel assembly (Item 3 in Fig. 2a) was installed. To simulate axial force applied on the side column, a self-equilibrium system (In Fig. 2b) was

designed. To measure the applied concentrated load, a load cell (Item 2 in Fig. 2a) was installed beneath the jack. The horizontal reaction force was measured by several tension/compression load cells (Item 5 in Fig. 2a) and load pin (Item 8 in Fig. 2a). The deflection of the beam and column was measured by a series of linear variable displacement transducers (LVDTs).

Experimental Results

Four PC beam-column sub-assemblies and two RC specimens (for reference) were tested by push-down loading regime. The comparison analysis was conducted to quantify the influences of location of column removal and strand profile on the disproportionate collapse resistance of PC frames. The key results were listed in Table 4 and discussed in the following sections.

Global Performance

Nonprestressed Specimen RCM

Fig. 3 shows the vertical load resistance versus the vertical removed column displacement (RCD). For RCM, at RCD of 30 mm, the yield load (YL), which was defined as the load when the first yielding start in longitudinal reinforcement, of 42 kN was obtained. Increasing the RCD to 70 mm, the first peak load (FPL) of 53 kN was recorded, which was 126% of that of YL. After FPL, because of concrete crushing, a load softening occurred with the increase of RCD. However, the re-ascending of load resistance was observed when the RCD reached 300 mm due to the mobilization of TCA. At RCD of 320 mm and 370 mm, rebar fracture was observed at the right side of the removed column, causing decrease of the load resistance by 15% and 23%, respectively. When the RCD reached 538mm, the load resistance sharply decreased by 28% due to rebar fracture. As the hydraulic jack reached its stroke capacity, test had to be stopped at RCD of 659 mm. The ultimate load (UL) at this stage was 79 kN.

As shown in Fig. 4, the rebar fracture and wide cracks were occurred in the beam end near

the removed column (BERC) while the compression zone of BERC suffered severe concrete crushing or spalling. Several penetrating cracks occurred in the beams while few cracks were observed in the joint.

Nonprestressed Specimen RCP

Specimen RCP has identical dimensions and reinforcement details as RCM, but no overhanging beam on the right side. As shown in Fig. 3, the YL of RCP was measured as 40 kN at a displacement of 27 mm. When the RCD further increased to 76 mm, the FPL of 51 kN was recorded, which was 96% of that of RCM. It indicates that the effects of boundary conditions on load resistance of RC frame is inconspicuous at the small deformation stage. The rebar fracture occurred in the beam end near the right side of the removed column at a RCD of 409 mm, but no rebar fracture occurred at the left side. The fracture of rebars resulted in a 28% reduction in the load resistance. The remaining rebars contributed to further development of TCA, resulting in re-raising of the load resisting capacity. Test was stopped when the RCD reached 665 mm, the UL of RCP was measured as 74 kN, which was lower than that of RCM only by 6%.

Fig. 5 shows the failure mode of RCP. In general, the failure mode of RCP was similar to RCM but more cracks formed in the right-side column.

PC Specimen PCM-S

Specimen PCM-S has identical details of nonprestressed rebar as RCM, but include two straight UPSs parallel to the beam axis (straight profile). As illustrated in Fig. 3, at a RCD of 30 mm, the YL of 68 kN was recorded. When the RCD reached 56 mm, the FPL of 79 kN, which was 49% higher than that of RCM, was recorded. When the RCD reached 179 mm, the applied load re-raised due to the involvement of TCA. With further increasing RCD to 463 mm, the load resistance increased again until rebar fracture. The UL of 228kN was measured at a RCD of 614 mm, which was 289% of that of RCM. Beyond this point, load resistance dropped sharply due to

the bottom strand fractured in the BERC.

Fig. 6 gives the failure mode of PCM-S. The fracture of rebars and the partial fracture of the bottom strand was observed in BERC. In the compression zone of the beam ends, severe concrete crushing was observed. A number of small flexural cracks and slight concrete crushing appeared in the side column without significant deformation. The penetrated flexural cracks were distributed along the beams, which indicated that the whole beam section was in tension at the stage of TCA.

PC Specimen PCP-S

As shown in Fig. 3, at the beginning of the test, the vertical load-RCD relationship of PCP-S is familiar to that of PCM-S. However, due to inadequate axial restraints, TCA in PCP-S could not be fully mobilized. The structural resistance increased gradually when the RCD exceeded 329 mm. The UL of 99 kN was obtained at a RCD of 499 mm. Thus, the UL and deformation capacity of PCP-S were 43% and 81% of those of PCM-S, respectively.

Unlike the PCM-S, the failure of PCP-S was governed by the pre-mature flexural-tension failure of the side column due to high lateral tensile load for side column. Thus, no strand was fractured. As shown in Fig. 7, the right-side column was subjected to severe inward deformation accompanied by an enormous number of flexural cracks. The bottom of the beam end near the right-side column was subjected to great compressive force, which resulted in the buckling of the rebar. Moreover, severe flexural/shear failure happened in the beam end near the right-side column. However, no penetrated cracks were formed in the beam, which indicates that majority of the tensile force of the beam was attributed to the strands, rather than the non-prestressed rebars.

PC Specimen PCM-P

Specimen PCM-P has similar reinforcement details as PCM-S, but only one UPS with parabolic profile was installed. As shown in Fig. 3 and Table 4, increasing the load to 43 kN, yielding was first observed in the BERC at a RCD of 27 mm. When the RCD reached 90 mm, the

FPL of 63 kN, which was 119% of that of RCM, was recorded. In conventional design, the parabolic UPS is expected to increase the hogging moment capacity of the beam ends. However, after removal of a column, the direction of bending moment at the beam end near the missing column changes from hogging into sagging. To this end, the parabolic UPS will induce additional sagging moment. In this test, the additional sagging moment led to pre-mature fracture of two bottom rebars at a RCD of 283 mm. The third fracture of the rebar occurred at a RCD of 567 mm, resulting in a 25% reduction in load resistance. When the MDC was further increased to 680 mm, the UL of 154 kN was measured, which was 195% of that of RCM.

Fig. 8 gives the failure mode of PCM-P, due to the additional sagging moment induced by parabolic strand, the damage at the BERC was more severe than that of PCM-S. However, damage at the beam end near the side column (BESC) was slighter comparing to PCM-S, which can be explained as the increased hogging moment capacity due to the parabolic UPS.

PC Specimen PCP-P

As shown in Fig. 3, the variation in trend of the load-displacement curve of PCP-P was similar to that of PCM-P in the test beginning. The FPL of the specimen was measured as 61 kN at a RCD of 66 mm. When the RCD increased to 353 mm, the first rebar fracture was observed in BERC, resulting in the decreasing of the applied load. When RCD was beyond 480 mm, the greater lateral deformation of the right column without overhanging beam slowed down the rise of the load resistance. When RCD increased to 600 mm, the UL of 86 kN was measured, which was 56% of that of PCM-P.

Fig. 9 demonstrates the failure mode of PCP-P. Similar to PCP-S, the right-side column was failed by eccentric tension with severe concrete crushing and flexural cracks. However, the main differences were the rebar fracture occurred in the BERC due to the additional sagging bending moment produced by the parabolic strand. Extensive tensile cracks developed over the whole

beam span, and some cracks even penetrated the beam cross-sections. Moreover, no shear failure was observed in the beam end due to the parabolic strand increased the compressive zone of the beam end section.

Horizontal Reaction Force

Fig. 10 shows the horizontal reaction force-RCD relationship. The horizontal reaction forces at each side are the summation of the horizontal reactions measured in the tension/compression load cells and load pin (shown in Fig. 2). Table 4 lists the maximum horizontal compressive and tensile reaction force. As shown in Fig. 10a, the maximum compressive reaction force of RCM was -99kN. The maximum compressive reaction forces on the left and right sides of RCP were -81kN and -69 kN, respectively. As shown in Fig. 10b, for PC specimens with the straight UPS, the compressive reaction force was reversed to tensile reaction force at a RCD much earlier than that of specimens with parabolic UPS, indicating that TCA was mobilized earlier in PC specimens with straight UPS.

The reaction of each horizontal restraint was denoted in Fig.11, in the small deformation stage, the majority of horizontal reaction was transferred from the bottom of the side column. However, in large deformation stage, the majority of the horizontal reaction force was provided by the overhanging beam. Moreover, the horizontal tension at the overhanging beam was most sensitive to the beam rebar fracture and the failure of the side column. Fig 11d shows the horizontal reaction at the right side of PCP-P, at the large deformation stage, the horizontal tension at the top constraint was greater than that at bottom one, which implicitly indicated that hogging moment still actively developed in the BENS.

Beam and Column Deformation

Fig. 12 illustrates the deformation of the beams in PCM-S and PCP-P. As shown in Fig. 12a,

the beams of PCM-S kept straight during the test, which agreed with the chord rotation well. For PCP-P, the deformation of beams was almost symmetric before the first fracture of the rebar at BERC. In the large deformation stage, the beam segment near the BERC experienced larger rotation than that near the BESC.

The lateral drift of the right-side column of the specimens was plotted in Fig. 13. As given in this figure, outward movement was measured at the initial stage due to the development of CAA in the beams. It can be found that the specimens with the straight UPS had larger inward movement than the specimens with the parabolic UPS for a given RCD. Due to absence of the overhanging beam, the right-side column of PCP-S and PCP-P experienced large inward movement in large deformation stage.

Strain Gauge Reading

Fig. 14 shows the strain gauge results. As shown in the figure, for Specimen PCM-S, initially, the longitudinal reinforcements experienced compressive strain. The bottom rebar near the removed column yielded first. Thus, plastic hinges were formed at each beam end at the CAA stage. The maximum compressive strain was recorded at the top rebar near the removed column and the bottom rebar near the side column, which agreed with the failure mode (refer to Fig. 6). At the TCA stage, the compressive strain of bottom reinforcement gradually decreased and finally transferred into tensile. At the ultimate load stage, no compressive strain was recorded at either the top or the bottom reinforcement, which indicates that all non-prestressed reinforcements contributed to TCA. In general, the strain gauge reading of PCM-P and PCP-P was similar to that of PCM-S. However, for PCP-S, compressive strain was measured at longitudinal reinforcements even at large deformation stage.

Variation of Prestressing Force in Strands

Fig. 15 illustrates the variation of the prestressing force of strands of the four specimens. As described in the previous section, the effective prestressing force of $0.65 f_{pu}$ (119 kN) was applied in each strand. However, due to the prestressing force loss, the effective prestressing force of PCM-S, PCP-S, PCM-P, and PCP-P was respectively measured as 230 kN, 228 kN, 111 kN, and 111kN, respectively, at the beginning of the test. As shown in Fig. 15a, the strand in PCM-P yielded at a RCD of 520 mm. However, the strand in PCP-P did not yield during the loading process, indicating that the strand was not fully utilized when the loss of a penultimate column was focused on. As shown in Figs. 15b and c, for PCM-S and PCP-S, the prestressing force of the bottom strand was similar to that of top strand. The bottom strand in PCM-S fractured at a RCD of 614 mm, and the maximum prestressing force was measured as 172 kN at this displacement. Moreover, it was found that the fracture of strand was observed before reaching its ultimate strength. This is because the strand was subjected to complex stress during the tests, rather than the pure tensile stress. In general, the fracture of strand occurred at the position with great stress concentration, such as the beam-column interfaces.

Discussion of the Results

The Effects of the Profile of UPS

As illustrated in Fig. 3 and Table 4, the measured FPL resistance of RCM, PCM-S, PCM-P, RCP, PCP-S, and PCP-P were 53 kN, 79 kN, 63 kN, 51 kN, 77 kN, and 61 kN. Compared to RCM, the FPL of PCM-S and PCM-P was increased by 49% and 19%, respectively. Compared with RCP, the FPL of PCP-S and PCP-P was increased by 51% and 20%, respectively. It was found that both straight and parabolic strand profiles can effectively increase the FPL of RC frames regardless the position of column removal. The UL resistance of RCM, PCM-S, and PCM-P was 79 kN, 228 kN,

and 154 kN, respectively. Compared with RCM, the UL resistance of PCM-S and PCM-P was increased by 189% and 95%, respectively. Similarly, compared with RCP, the FPL resistance of PCP-S and PCP-P was increased by 34% and 16%, respectively. It was found that both strand profiles can effectively increase the UL resistance, especially for the specimens subjected to the loss of an interior column scenario.

As given in Fig. 3, PC specimens with parabolic UPS achieved greater deformation capacity (the displacement at UL) than those with straight UPS. Under scenario of middle column removal, the boundary condition allowed the UPS to sufficiently develop tensile force; the straight UPS further produced larger elongation compared with the parabolic one at the same displacement, resulting in earlier fracture of the UPS. Therefore, PCM-S had the lower deformation capacity compared with PCM-P. In comparison, the failure of PC specimen under penultimate column removal scenario was controlled by eccentric tension failure of the side column. Thus, the lower deformation capacity of PCP-S compared with PCP-P can be attributed to the greater tensile forces developed in the straight UPS, which aggravates the second order effect in the side column.

The Effects of the Position of Column Removal

As presented in Fig. 3 and Table 4, the FPL resistance of RCM and RCP was 53 kN and 51 kN, respectively. The UL resistance of RCM and RCP was 79 kN and 74 kN. Thus, compared with RCP, the FPL and UL of RCM increased by 4% and 7%, respectively. Moreover, RCM and RCP had similar deformation capacity. Therefore, the position of column removal had limited influences on the performance of RC frame to resist disproportionate collapse.

The FPL of PCM-S, PCP-S, PCM-P, and PCP-P was 79 kN, 77 kN, 63 kN, and 61 kN. Therefore, at relatively small deformation stage, the position of column removal had little influences on the load resistance of the PC specimens. However, the UL of PCM-S, PCP-S, PCM-P, and PCP-P was 228 kN, 99 kN, 154 kN, and 86 kN, respectively. The UL of PCM-S was 130%

higher than PCP-S, while the UL of PCM-P was 79% higher than PCP-P. Thus, the UL capacity of the PC specimen was significantly influenced by the position of column removal. In addition, due to absence of the overhanging beam, the right-side column of PCP-S and PCP-P suffered severe flexural tension failure due to large eccentricity, resulting in lower deformation capacity compare with PCM-S and PCM-P.

In summary, the position of column removal not only affected the UL capacity but also deformation capacity of the PC specimens.

Dynamic Resistance

As discussed above, the UPS effects on the quasi-static response of PC frame in resisting disproportionate collapse had been captured by the experimental results. However, disproportionate collapse is a dynamic event, and therefore, it is important to investigate the dynamic behavior of these specimens. An energy-based method proposed by Izzuddin et al. (2008) was adopted in describing the dynamic evaluation. In their method, the external work is assumed to be totally converted to strain energy in the remaining building if a new balance can be achieved. This method is mathematically expressed as

$$P_d(u_d) = \frac{1}{u_d} \int_0^{u_d} P_{qs}(u) du \quad (1)$$

where $P_d(u)$ and $P_{qs}(u)$ are the dynamic load resistance and the quasi-static load resistance at specific displacement demand u .

Fig. 16 illustrates the dynamic capacity curves of the specimens with and without UPS. The dynamic ultimate load of Specimen RCM, RCP, PCM-S, PCM-P, PCP-S, and PCP-P were 48 kN, 44 kN, 113 kN, 79 kN, 80 kN, and 62 kN, respectively. Thus, the straight and parabolic UPSs increased the ultimate dynamic load of RCM by 135% and 65%, respectively. Similarly, the straight and parabolic UPSs increased the dynamic ultimate load of RCP by 82% and 41%,

respectively.

Bending Moment of the Right-Side Column

To better understand the failure mode of the right column, the bending moment of critical section E-E in the right column was determined by Eq. (2) and shown in Fig. 17.

$$M_E = H_4 L_0 + V_1 \Delta \quad (2)$$

where H_4 is the horizontal reaction force in the top horizontal constraint; L_0 is the length from the top horizontal constraint to section E-E; V_1 is the designed axial compressive force of 703 kN on the side column; Δ is horizontal movement in Section E-E.

Fig. 17 shows the variation of bending moment in right-side column of the PC frame under a penultimate column removal scenario while Fig. 18 presents the theoretical M-N curve of E-E section. As shown in Fig. 17, the bending moment at Section E-E was negative (clockwise direction) first and then converted to positive (counter-clockwise direction). When the RCD reached 329 mm, the bending moment of E-E section was 76 kN·m and then began to decrease. Theoretically, as shown in Fig. 18, the E-E section reached eccentric tension failure at this stage. However, the re-ascending behavior was observed for the bending moment. This is because the designed axial compression force in the side column was assumed to be constant in calculation, but actually it kept decreasing after damage in the side column. Similar observation was found in PCP-P.

De-composition of the Load Resistance

Fig. 19 illustrates the static equilibrium of a section of a deformed beam. As given in the figure, the vertical load resistance consists of the vertical component of axial force and shear force, which can be mathematically expressed by:

$$P = \sum_{j=1}^2 (N_j \sin \theta_j + V_j \cos \theta_j) \quad (3)$$

where P is the applied load; N_j and V_j are the axial force and shear force transferred from the beams to the beam-column interfaces, respectively; θ_j is the rotation of the beam section.

Fig. 20 shows the de-composition of the load resistance at the critical section (beam-removed column interface) of the PC specimens. All those PC specimens had similar load resistance component at the beginning of the test. At this stage, the shear force (bending moment) contributed majority of the load resistance, the axial force made negative but marginal contribution. At large deformation stage, the contribution from the shear force of PCM-S and PCM-P decreased quickly and even became negative at the end of the tests, while the axial force contributed majority of the load resistance. Thus, the TCA from strand was the main load-resisting mechanism at the large deformation stage. In comparison, the contribution from the shear force of PCP-S is always greater than that from the axial force, indicating that bending moment still actively developed in the BENM (no rebar fracture occurred). Regarding PCP-P, due to rebar fracture at the BENM, the contribution from the shear force was much lower compared with PCP-S.

In general, two major load-resisting mechanisms were found from the PC specimens to resist the applied load: beam action and TCA. The beam action can be further categorized as the flexural action and CAA depend on whether axial compressive force developed in the beams. Firstly, the beams deformed within elastic range without axial forces developed in the beams, the applied load was resisted by the bending of beam ends. Subsequently, the plastic hinges began to form in the beam ends due to increased deflection, while the axial compressive force began to develop in the beams because the beam ends prone to move outward but were constrained by boundary. With the help of the induced axial compressive forces, the bending moment capacity of the beam ends exceeded yield bending moment. This is the so call “CAA”. Therefore, the enhancement of the flexural capacity due to CAA was inherently attributed to additional plastic moment caused by the axial compressive forces in the beams. When the beams undergo the deformation of approximate

one beam depth, the axial compressive force began to transfer to axial tensile force. After that, the TCA began to progress to resist the applied load.

Conclusions

In this study, four posttensioned concrete (PC) frames and two referential reinforced concrete (RC) specimens were tested subjected to push-down loading regime. Based on experimental and analytical results, the conclusions were drawn as follows:

1. The unbonded posttensioning strand (UPS) can significantly increase the load resistance, comparing to conventional RC specimen. However, the UPS induced considerable tensile force to side column may lead to flexural tension failure due to large eccentricity of the side column. Thus, the potential enlarged collapse zone for PC frames due to greater horizontal tensile force for side columns should be considered seriously.
2. The position of column removal had a minor effect on the performance of RC frame. For PC specimens, the position of column removal had limited effects on the first peak load (FPL). However, it had considerable effects on their UL capacity. This is mainly because considerable tensile catenary action (TCA) could develop in PC beams with the loss of a middle column. Conversely, TCA could not be fully developed in PC beams when the loss of a penultimate column was considered as the side column prone to occur eccentric tension failure.
3. PC specimen with straight strand profile achieved greater load resistance compared with those with parabolic strand profile due to greater strand area. When consideration of the loss of a penultimate column, PC specimen with straight strand profile may accumulate the internal damage of column due to greater tensile force required at identical displacement stage. When the loss of a middle column was considered, the straight strands were fractured earlier than the parabolic ones, since the straight strands experienced lager elongation than the parabolic one

at the same vertical displacement.

4. The load resistance de-composition analysis shows that the load resistance component of each PC specimen at small deformation stage was similar; meanwhile, the shear forces (bending moments) contributed most of the load resistance while axial force made negative contribution. However, the load resistance from axial forces dominated the load resistance at large deformation stage except PCP-S. In other words, for PC specimens, the beam action (flexural action together with CAA) and TCA are the main load-resisting mechanism at small and large deformation stage, respectively.

Data Availability

Some or all data, models, or code that support the findings of this study are available from the corresponding author upon reasonable request.

Acknowledgements

This research was supported by a research grant provided by the Natural Science Foundation of China (Nos. 52022024, 51778153), Guangxi Science and Technology Base and Special Fund for Talents Program (Grant Nos. Guike AD20159011). Any opinions, findings and conclusions expressed in this paper are those of the writers and do not necessarily reflect the view of Natural Science Foundation of China and Guangxi Science and Technology Base and Special Fund for Talents Program.

REFERENCES

- ACI Committee 318. "Building Code Requirements for Structural Concrete (ACI 318-14) and Commentary (318R-14)." American Concrete Institute, Farmington Hills, MI, 433 pp; 2014.
- Deng, X. F., Liang, S. L., Fu, F., and Qian, K. (2020). "Effects of high-strength concrete on

progressive collapse resistance of reinforced concrete frame.” *J. Struct. Eng.*, 146(6): 04020078.

Department of Defense (DoD). (2016). “Design of buildings to resist progressive collapse.” *Unified Facilities Criteria (UFC) 4-023-03*, Washington, DC.

Ellingwood B. R. (2006). Mitigating risk from abnormal loads and progressive collapse. *Journal of Performance of Constructed Facilities*, 20(4): 315-323.

FarhangVesali, N., Valipour, H., Samali, B., and Foster, S. (2013). “Development of arching action in longitudinally-restrained reinforced concrete beams.” *Constr. Build. Mater.*, 47: 7-19.

General Services Administration (GSA). (2013). “Progressive collapse analysis and design guidelines for new federal office buildings and major modernization projects.” Washington, DC.

Husain, M., Yu, J., Osman, B. H., and Ji, J. (2021). “Progressive collapse resistance of post-tensioned concrete beam-column assemblies under a middle column removal scenario.” *J. Build. Eng.*, 34: 101945.

Izzuddin, B. A., Vlassis, A. G., Elahazouli, A. Y., and Nethercot, D. A. (2008). “Progressive collapse of multi-story buildings due to sudden column loss-Part 1: simplified assessment framework.” *Eng. Struct.*, 30(5): 1308-1318.

Ma, F. H., Gilbert, B. P., Guan, H., Lu, X. Z., and Li, Y. (2020). “Experimental study on the progressive collapse behaviour of RC flat plate substructures subjected to edge-column and edge-interior column removal scenarios.” *Eng. Struct.*, 209:110299.

Keyvani, L. and Sasani, M. (2015). “Analytical and experimental evaluation of progressive collapse resistance of a flat-slab posttensioned parking garage.” *J. Struct. Eng.* 141: 1–8.

Keyvani, L. and Sasani, M. (2016). “Response of a post-tensioned floor following a column loss.” *ACI Struct. J.*, 309: 1–18.

- Lu X. Z., Lin, K. Q., Li, Y., Guan, H., Ren, P. Q., and Zhou, Y. L. (2017) "Experimental investigation of RC beam-slab substructures against disproportionate collapse subject to an edge-column removal scenario." *Eng. Struct.*, 149: 91-103.
- Nimse, R. B., Joshi, D. D., and Oatel, P. V. (2014) "Behavior of wet precast beam column connections under progressive collapse scenario: an experimental study." *Int J Adv. Struct. Eng.*, 6 (4):149–59.
- Orton, S., Jirsa, J. O., and Bayrak, O. (2009). "Carbon fiber-reinforced polymer for continuing in existing reinforced concrete buildings vulnerable to collapse." *ACI Struct. J.*, 106(5): 608-616.
- Pham, X. D. and Tan, K. H. (2014). "Experimental response of beam-slab substructures subject to penultimate-external column removal." *J. Struct. Eng.*, 141(7), 04014170.
- Peng, Z. H., Orton, S. L., Liu, J. R., and Tian, Y. (2018). "Experimental study of dynamic progressive collapse in flat-plate buildings subjected to exterior column removal" *J. Struct. Eng.*, 143(9), 04017125.
- Qian, K., Hu, H. N., Weng, Y. H., and Deng, X. F. (2020). "Numerical investigation on load transfer mechanism of bonded post-Tensioned concrete beam-column substructures against progressive collapse." *Adv. Struct. Eng.*, 6:136943322098165.
- Qian, K. and Li, B. (2019). "Investigation into resilience of precast concrete floors against progressive collapse." *ACI Struct. J.*, 116(2): 171-182.
- Qian, K., Liu, Y., Yang, T., and Li, B. (2018). "Progressive collapse resistance of posttensioned concrete beam-column subassemblages with unbonded posttensioning strands." *J. Struct. Eng.*, 144: 4017182.
- Qian, K., Zhang, X. D., Fu, F., and Li, B. (2019). "Progressive collapse-resisting mechanisms of planar prestressed concrete frame." *ACI Struct. J.*, 116(4): 77-90.
- Qian, K., Liang, S. L., Fu, F., and Li, Y. (2021). "Progressive collapse resistance of emulative

precast concrete frames with various reinforcing details.” *J. Struct. Eng.*, 147(8): 04021107.

Sasani, M., Bazan, M., and Sagioglu, S. (2007). “Experimental and analytical progressive collapse evaluation of actual reinforced concrete structure.” *ACI Struct. J.*, 104(6): 731-739.

Sheffield, C., Audrey, K., and Hoon, V. N. P. (2011). “An instrumented full-scale building disproportionate collapse test.” Proceedings of 14th international symposium on interaction of the effects of munitions with structures 2011. Seattle, Washington.

Su, Y. P., Tian, Y., and Song, X. S. (2009). “Progressive collapse resistance of axially-restrained frame beams.” *ACI Struct. J.*, 106(5):600–7.

Tian, Y., Lin, K. Q., Lu, X. Z., Zhang, L., Li, Y., and Guan, H. (2020). “Experimental and theoretical study of seismic and progressive collapse resilient composite frames.” *Soil Dynamics and Earthquake Engineering*, 139:106370

Xiao, Y., Kunnath, S., Li, F. W., Zhao, Y. B., Lew, H. S., and Bao, Y. (2015). “Collapse test of three-story half-scale reinforced concrete frame building.” *ACI Struct. J.*, 112(4): 429-438.

Yi, W. J., He, Q. F., Xiao, Y., and Kunnath, S. K. (2008). “Experimental study on disproportionate collapse-resistant behavior of reinforced concrete frame structures.” *ACI Struct. J.*, 105(4): 433-439.

Yu, J., Rinder, T., Stolz, A., Tan, K. H., and Riedel, W. (2014). “Dynamic progressive collapse of an RC assemblage induced by contact detonation.” *J. Struct. Eng.*, 140 (6): 04014014.

Yu, J. and Tan, K. H. (2013a). “Experimental and numerical investigation on progressive collapse resistance of reinforced concrete beam column sub-assemblages.” *Eng. Struct.* 55(1): 90-106.

Yu, J., Tan and K. H. (2013 b). “Structural Behavior of Reinforced Concrete Beam-Column Sub-Assemblages under a Middle Column Removal Scenario.” *J. Struct. Eng.*, 139(2): 233-50.

Yu, J., Tang, J. H., and Luo, L. Z. (2020). “Effect of boundary conditions on progressive collapse resistance of RC beam-slab assemblies under edge column removal scenario”, *Eng. Struct.*,

225(15): 111272.

Zhou, Y., Chen T. P., Pei, Y. L., Hwang, H.J., Hu, X., Yi, W. J., and Deng, L. (2019). “Static load test on progressive collapse resistance of fully assembled precast concrete frame structure.”

Eng. Struct., 200:109719

Zhou Y., Yang, J. B., Wang, Z. S., Hwang, H. J., Huang, Y., Deng, L., and Yi, W. J. (2021). “Static Load Test on the Progressive Collapse Resistance of Precast Concrete Frame Substructure

during and after High Temperature.” *J. Struct. Eng.*, 147(8): 04021110.

FIGURE CAPTIONS

Fig. 1. Specimen detailing: (a) RCM; (b) PCM-S; (c) PCM-P

Fig. 2. Experimental setup: (a) photo of PCM-S; (b) drawing of PCM-S; (c) drawing of PCP-P

Fig. 3. Comparison of load-displacement curves

Fig. 4. Failure mode of Specimen RCM

Fig. 5. Failure mode of Specimen RCP

Fig. 6. Failure mode of Specimen PCM-S

Fig. 7. Failure mode of Specimen PCP-S

Fig. 8. Failure mode of Specimen PCM-P

Fig. 9. Failure mode of specimen PCP-P

Fig. 10. Horizontal reaction versus the RCD: (a) RC specimens; (b) PC specimens

Fig. 11. Contribution of the horizontal reaction of different measuring points: (a) RCM; (b) PCM-S; (c) Left side of PCP-P; (d) Right side of PCP-P

Fig. 12. Deformation of beams at various stages: (a) PCM-S; (b)PCP-P

Fig. 13. Horizontal drift in right-side column: (a) PCM-S; (b)PCP-S; (c) PCM-P; (d)PCP-P

Fig. 14. Strain of beam longitudinal rebar: (a) top rebar in PCM-S; (b) bottom rebar in PCM-S; (c) top rebar in PCP-S; (d) bottom rebar in PCP-S; (e) top rebar in PCM-P; (f) bottom rebar in PCM-P; (g) top rebar in PCP-P; (h) bottom rebar in PCP-P

Fig. 15. Prestressing force of tendons versus RCD: (a) Total prestressing force of the PC specimens; (b) PCM-S; (c) PCP-S

Fig. 16. Dynamic resistance of tested specimens

Fig. 17. The varying of bending moment in E-E section of side column

Fig. 18. Determination of the failure mode of PC specimens under penultimate column removal

Fig. 19. Determination of internal forces

Fig. 20. De-composition of the vertical resistance: (a) PCM-S; (b) PCM-P; (c) PCP-S; (d) PCP-P

Table 1. Details of Prototype Building and Corresponding Test Model

| Test Specimen | Prototype Building | | | Test model | | |
|---------------|----------------------------|------------------------------|---------------------|----------------------------|------------------------------|---------------------|
| | Beam (mm ²) | Column (mm ²) | Strand Size (mm) | Beam (mm ²) | Column (mm ²) | Strand Size (mm) |
| RCM | 500×300 | 500×500 | N/A | 250×150 | 250×250 | N/A |
| RCP | 500×300 | 500×500 | N/A | 250×150 | 250×250 | N/A |
| PCM-S | 500×300 | 500×500 | 17.8 | 250×150 | 250×250 | 12.7 |
| PCM-P | 500×300 | 500×500 | 17.8 | 250×150 | 250×250 | 12.7 |
| PCP-S | 500×300 | 500×500 | 17.8 | 250×150 | 250×250 | 12.7 |
| PCP-P | 500×300 | 500×500 | 17.8 | 250×150 | 250×250 | 12.7 |

Table 2. Specimen Characteristics

| Test Specimen | Effective prestressing | Axial compressive ratio | Beam reinforcements | | | | Position of removed column | Posttensioning strands profile |
|---------------|------------------------|-------------------------|---------------------|--------|------------------|--------|----------------------------|--------------------------------|
| | | | End section | | Mid-span section | | | |
| | | | Top | Bottom | Top | Bottom | | |
| RCM | N/A | 0.31 | 3T12 | 2T12 | 2T12 | 2T12 | Middle | N/A |
| RCP | N/A | 0.31 | 3T12 | 2T12 | 2T12 | 2T12 | Penultimate | N/A |
| PCM-S | $0.65 f_{pu}$ | 0.31 | 3T12 | 2T12 | 2T12 | 2T12 | Middle | Straight |
| PCM-P | $0.65 f_{pu}$ | 0.31 | 3T12 | 2T12 | 2T12 | 2T12 | Penultimate | Parabolic |
| PCP-S | $0.65 f_{pu}$ | 0.31 | 3T12 | 2T12 | 2T12 | 2T12 | Middle | Straight |
| PCP-P | $0.65 f_{pu}$ | 0.31 | 3T12 | 2T12 | 2T12 | 2T12 | Penultimate | Parabolic |

Note: f_{pu} equals to 1860 MPa, is the nominal ultimate strength of the tendons. T12 denotes deformed rebar with diameter of 12 mm.

536

537

538

539

540

Table 3. Material Properties of Tendon and Rebar

| Item | Nominal diameter (mm) | Yield strength (MPa) | Ultimate strength (MPa) | Elastic modulus (MPa) | Elongation (%) |
|---------|-----------------------------|----------------------------|-------------------------------|-----------------------------|-------------------|
| Strands | 12.7 | 1649 | 1970 | 213000 | 6.3 |
| R6 | 6 | 368 | 485 | 162000 | 20.1 |
| T12 | 12 | 462 | 596 | 171000 | 14.7 |
| T16 | 16 | 466 | 604 | 182000 | 17.0 |

541 Note: R6 denotes plain rebar with diameter of 6 mm while T12 and T16 denotes deformed rebar with diameter of 12
542 mm and 16 mm, respectively.

543

544

545

546

547

548

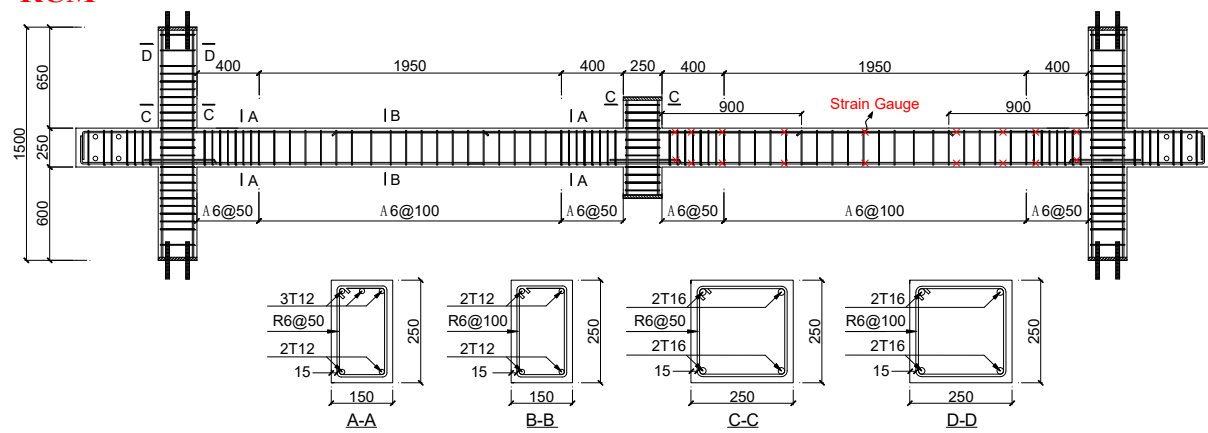
549

550

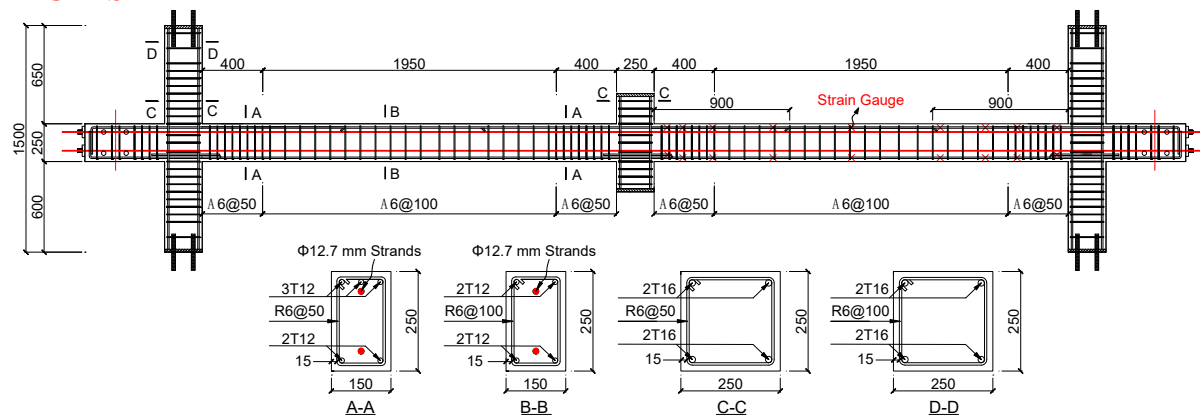
Table 4. Critical Results

| Test ID | Critical displacement (mm) | | | Critical load (kN) | | | MHCF in the left/ right side (kN) | MHTF in the left/ right side (kN) |
|---------|----------------------------|--------------------|------------------|--------------------|--------------------|------------------|---|---|
| | Yield load | First peak load | Ultimate load | Yield load | First peak load | Ultimate load | | |
| RCM | 30 | 70 | 659 | 42 | 53 | 79 | -99 | 167 |
| RCP | 27 | 76 | 665 | 40 | 51 | 74 | -81/-69 | 153/143 |
| PCM-S | 30 | 56 | 614 | 68 | 79 | 228 | -62 | 488 |
| PCM-P | 27 | 90 | 680 | 43 | 63 | 154 | -80 | 298 |
| PCP-S | 25 | 48 | 499 | 64 | 77 | 99 | -61/-61 | 162/122 |
| PCP-P | 19 | 66 | 600 | 39 | 61 | 86 | -87/-78 | 166/152 |

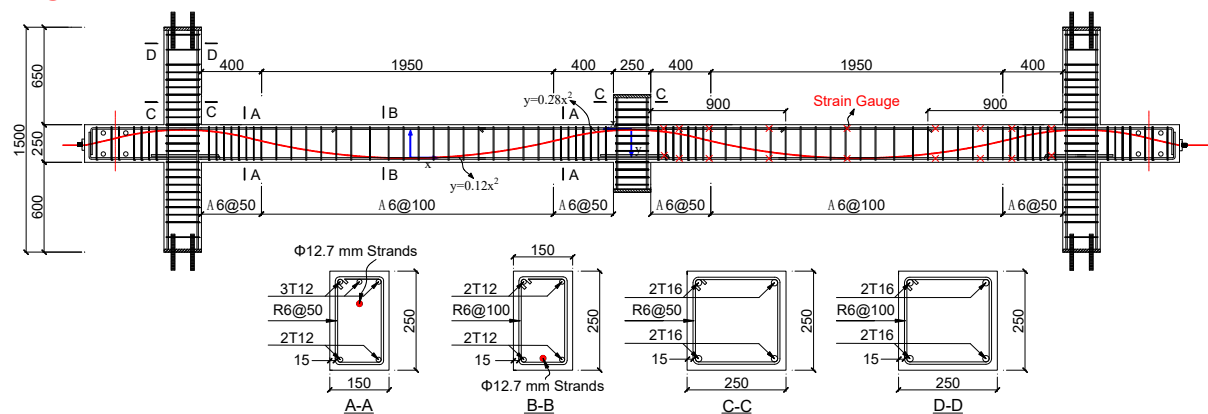
551 Note: MHCF and MHTF denote maximum horizontal compressive force and maximum horizontal tensile force,
552 respectively.

RCM

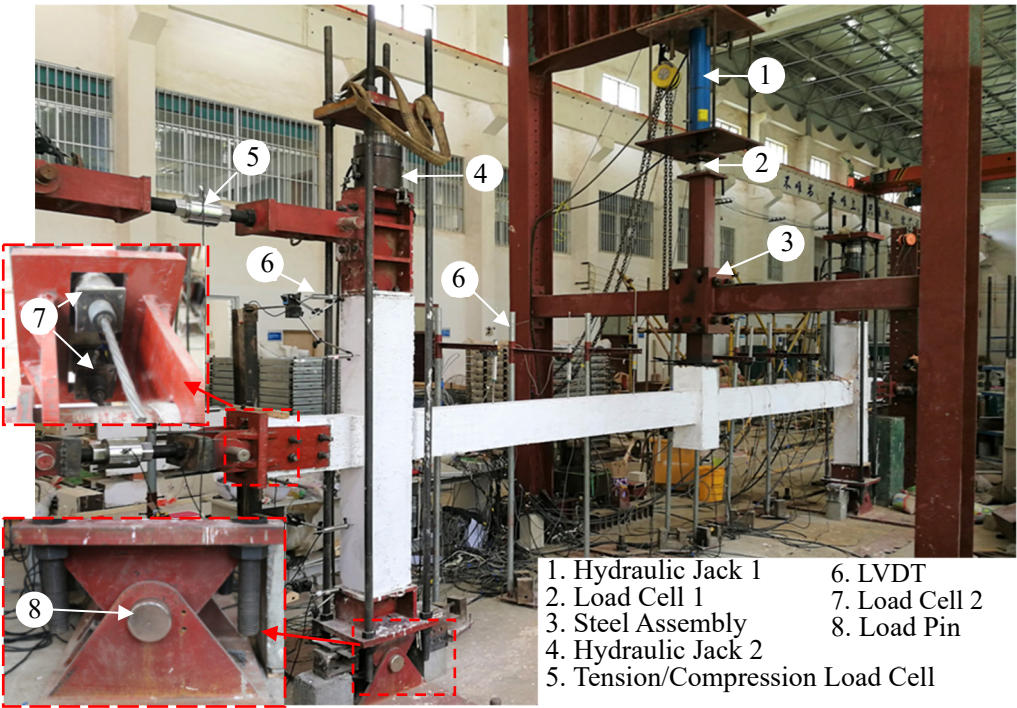
(a)

PCM-S

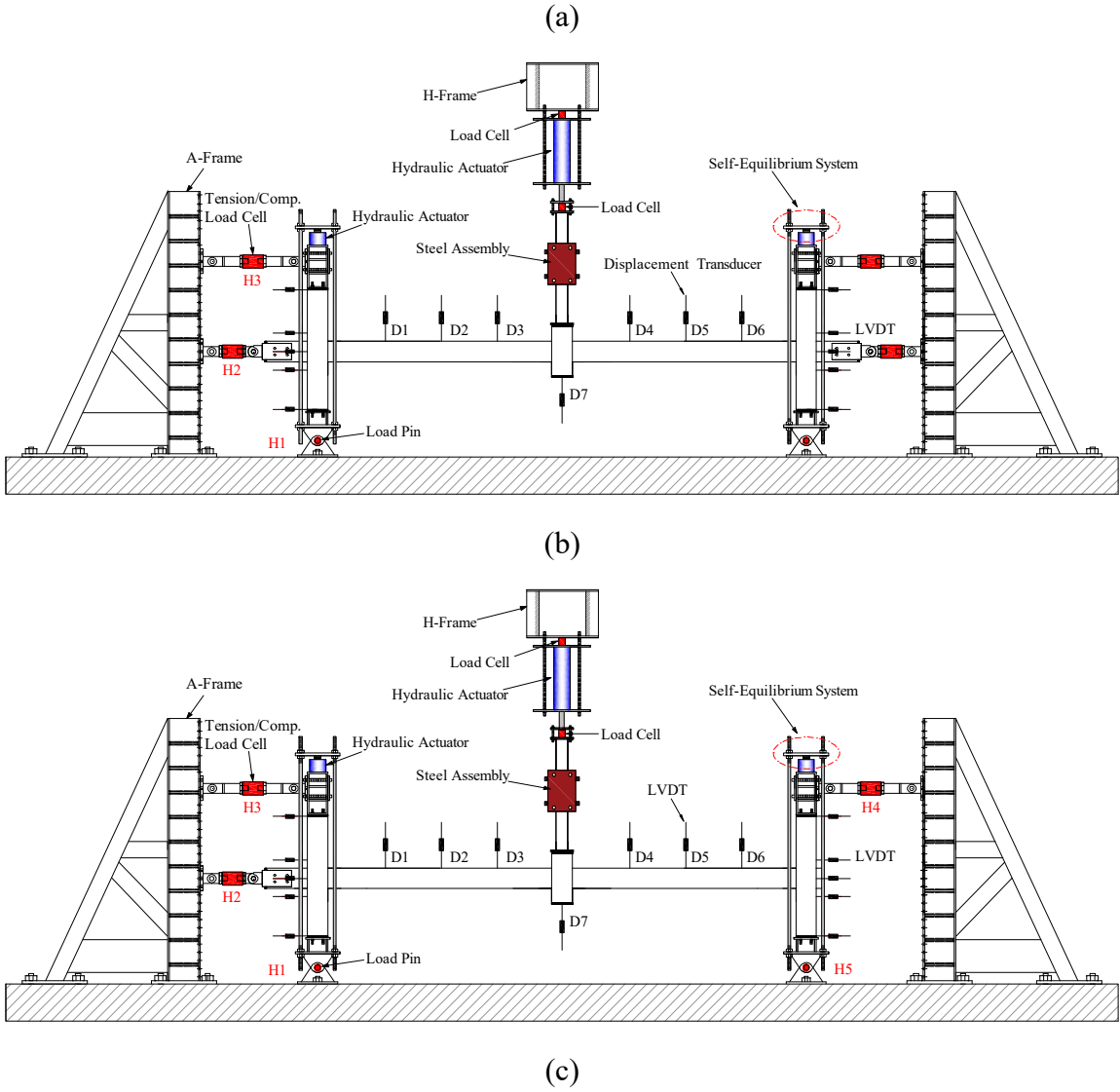
(b)

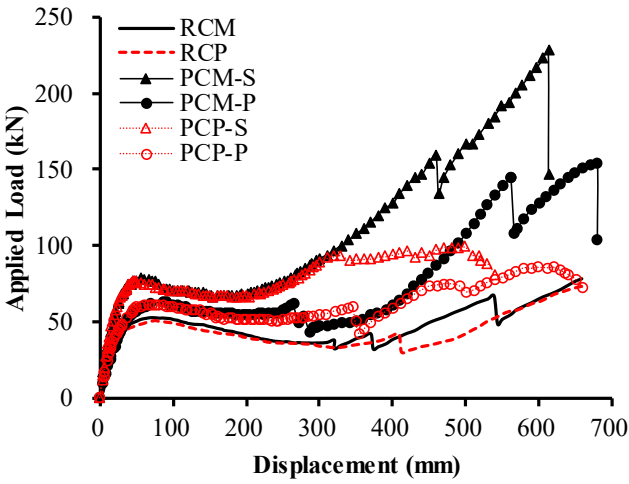
PCM-P

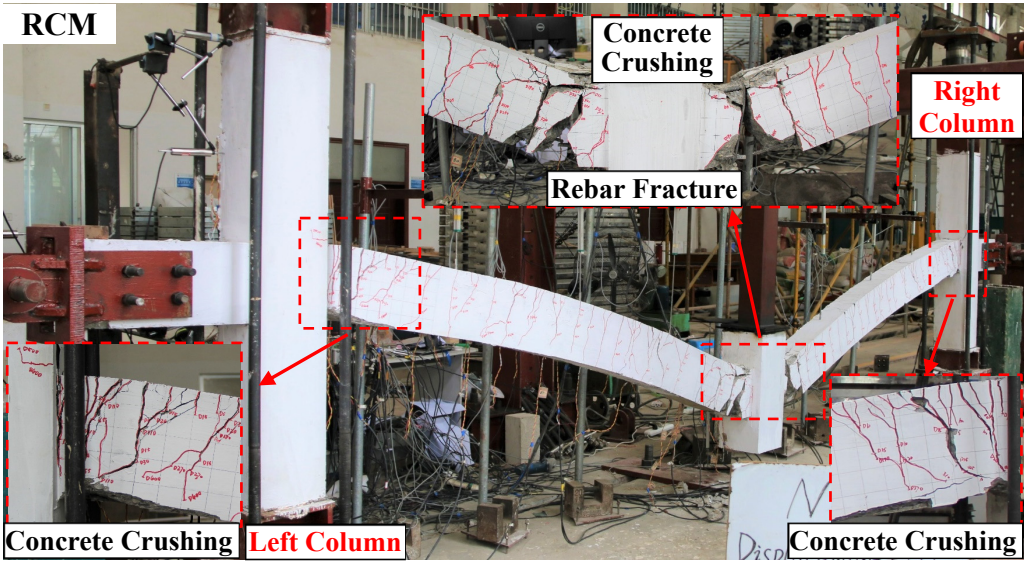
(c)

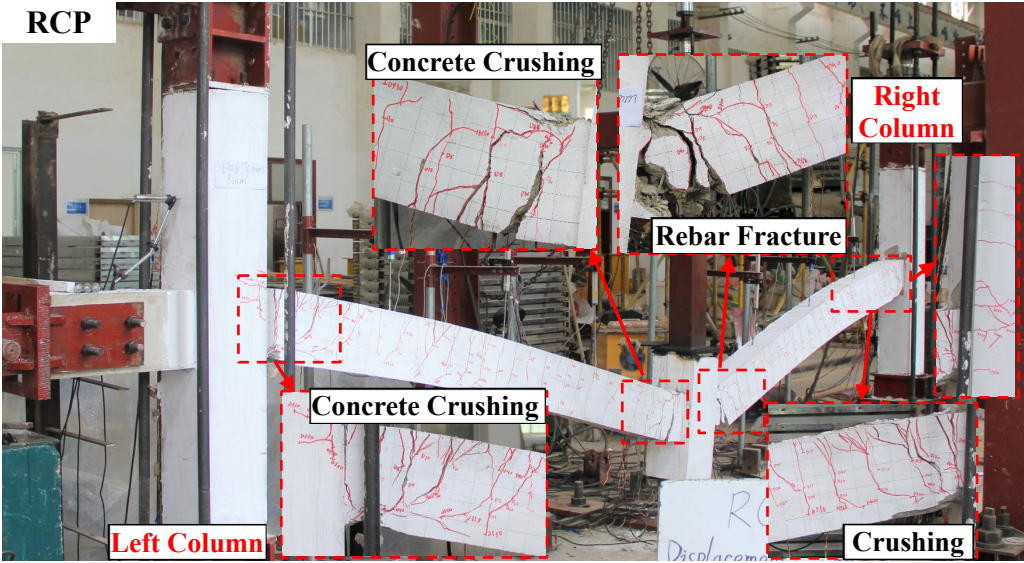


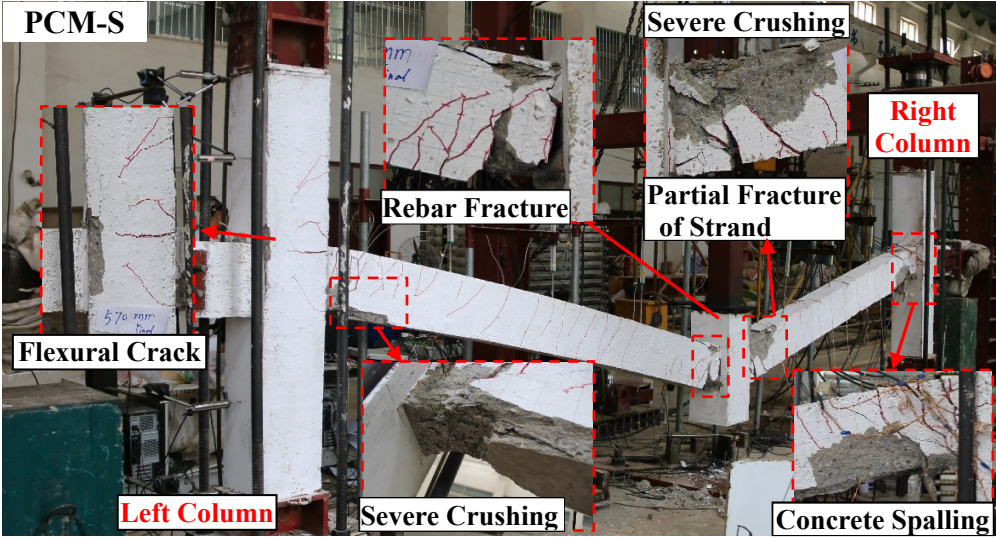
- 1. Hydraulic Jack 1
- 2. Load Cell 1
- 3. Steel Assembly
- 4. Hydraulic Jack 2
- 5. Tension/Compression Load Cell
- 6. LVDT
- 7. Load Cell 2
- 8. Load Pin

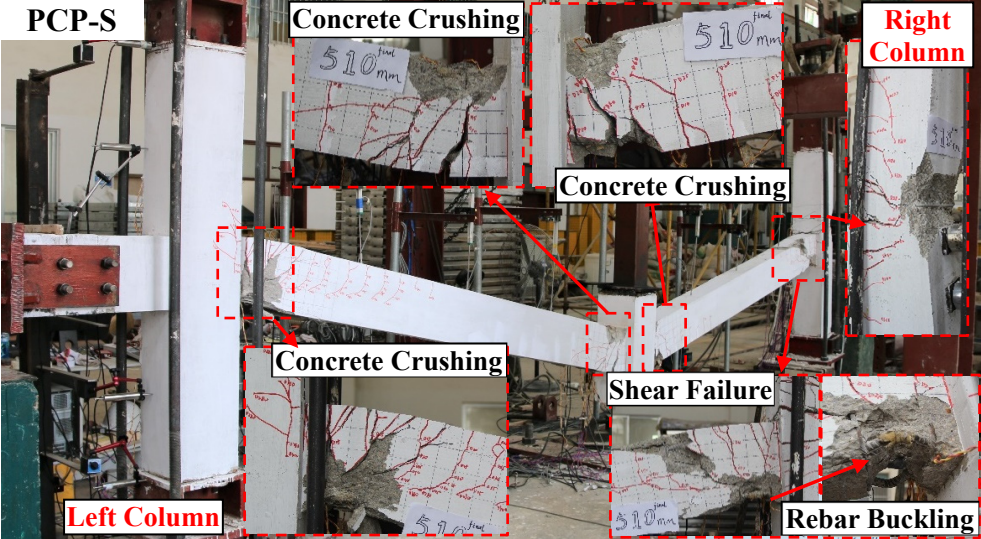


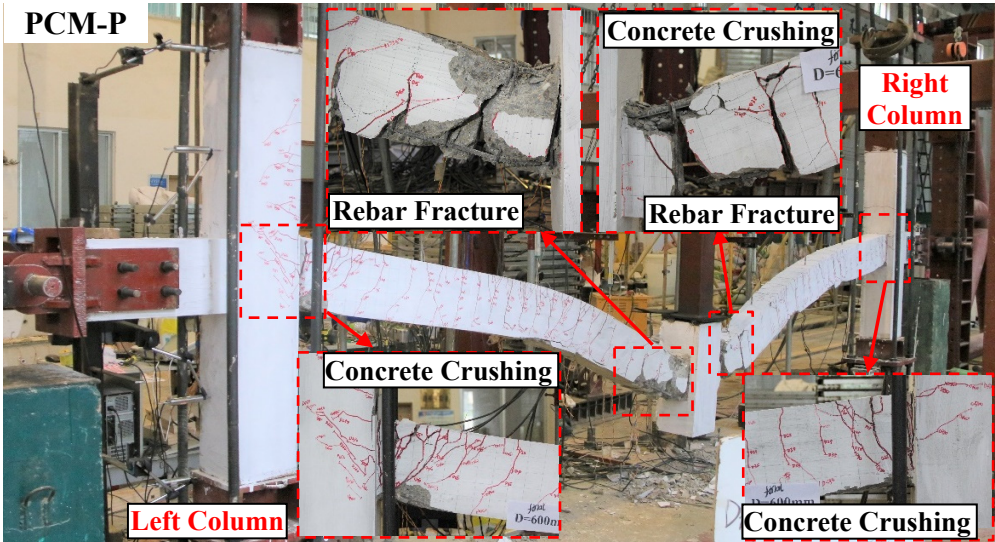


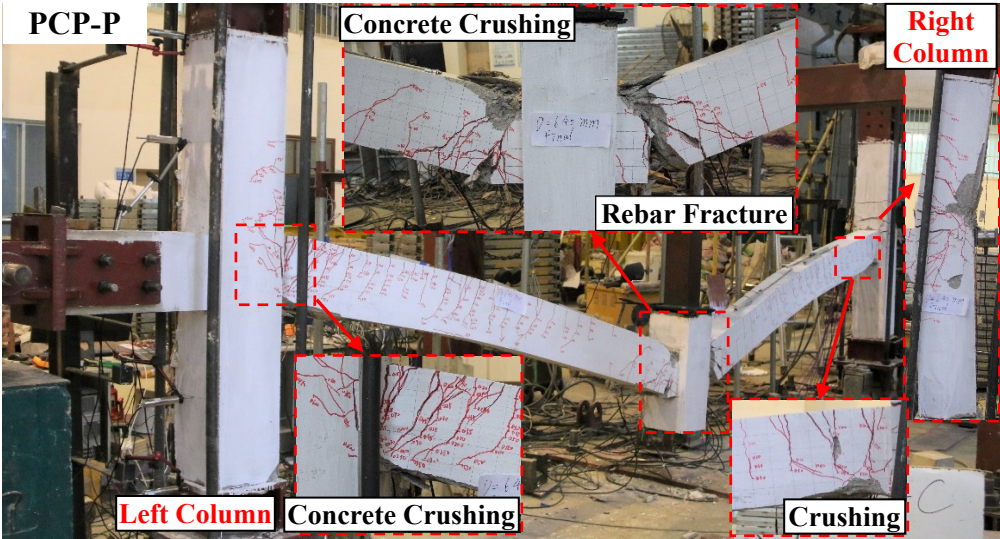


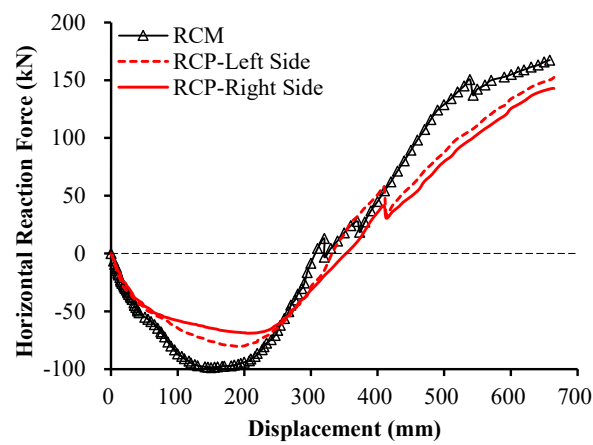




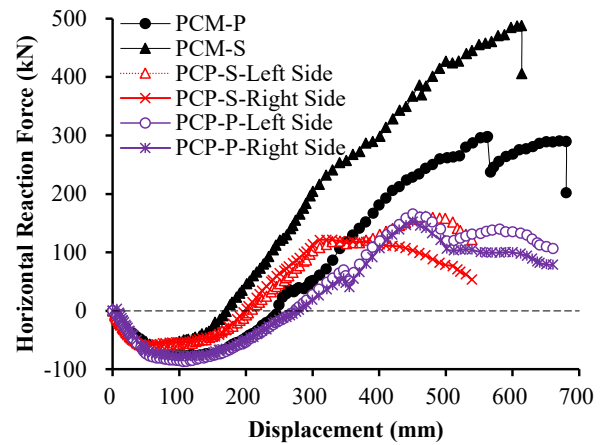




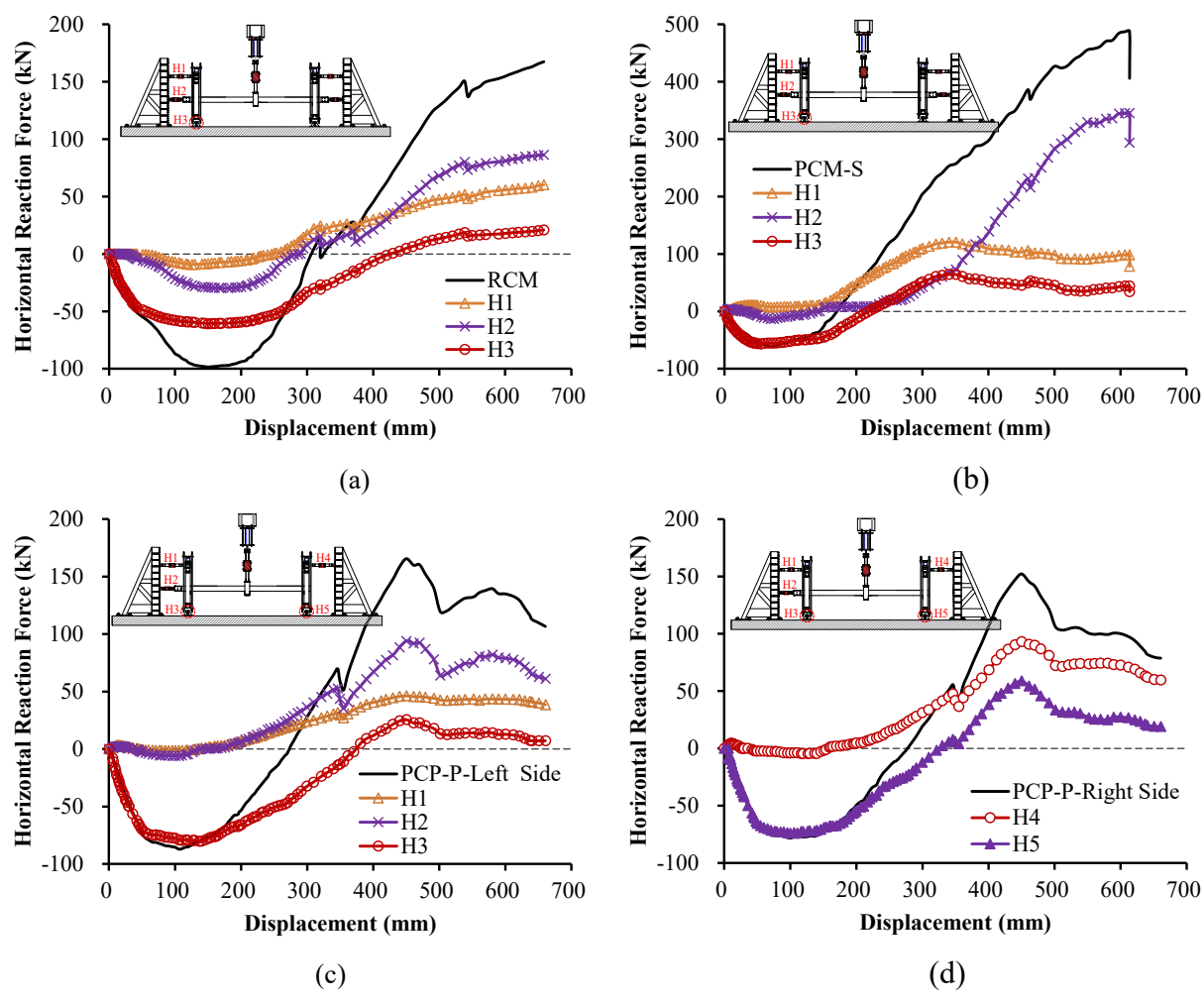


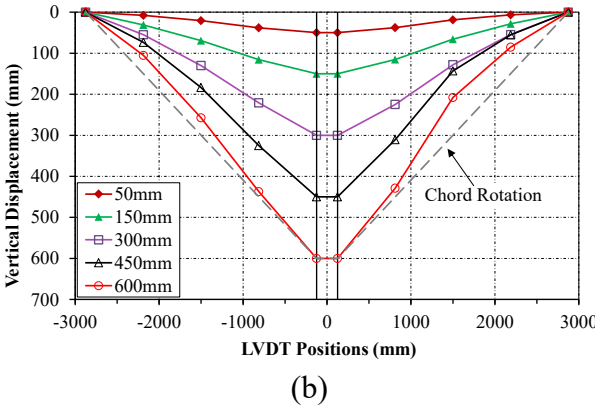
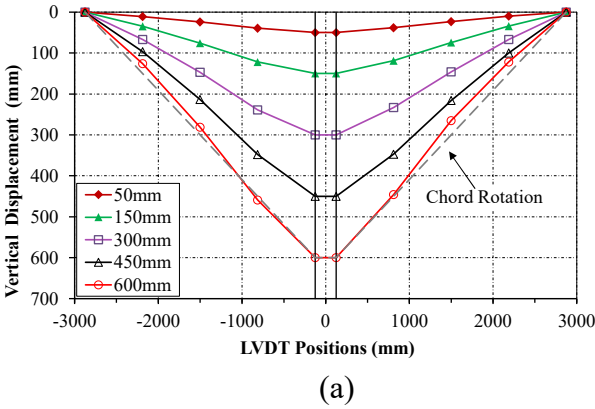


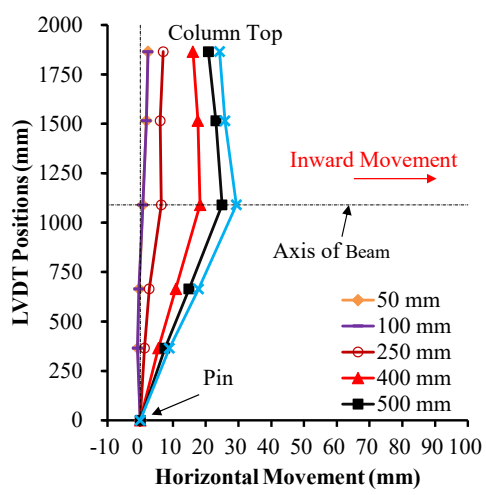
(a)



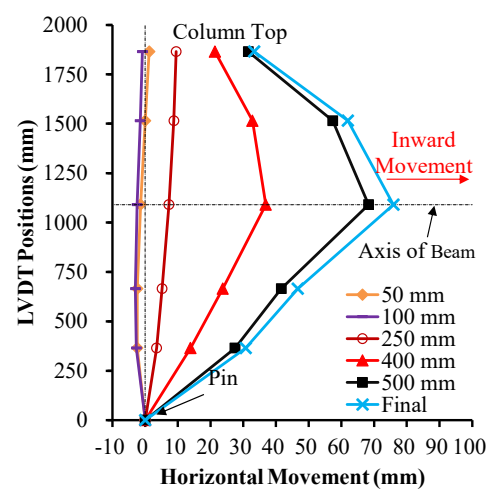
(b)



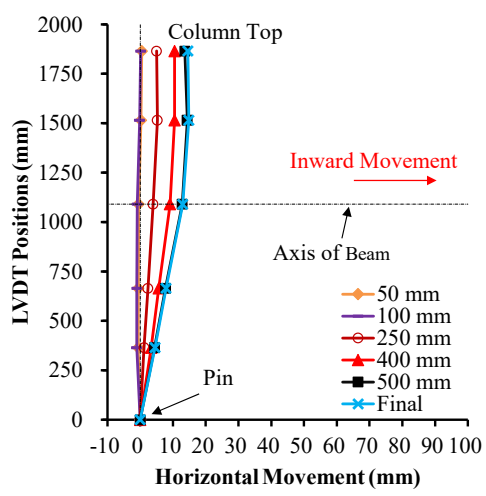




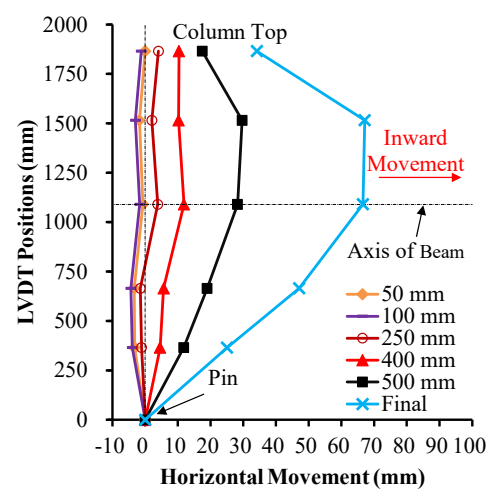
(a)



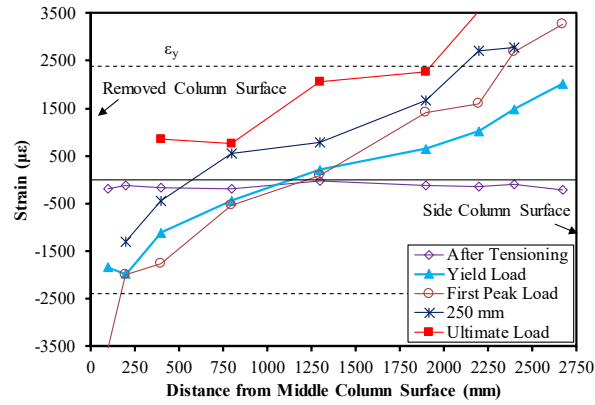
(b)



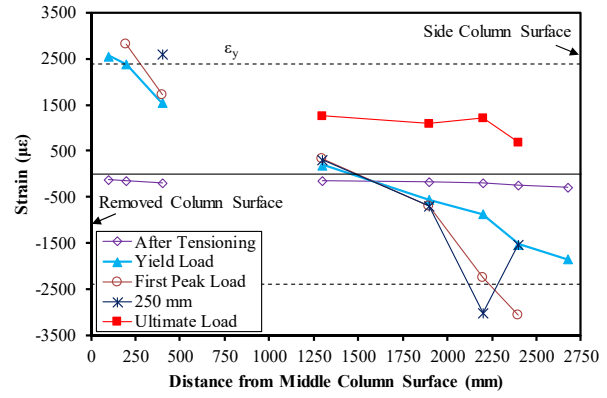
(c)



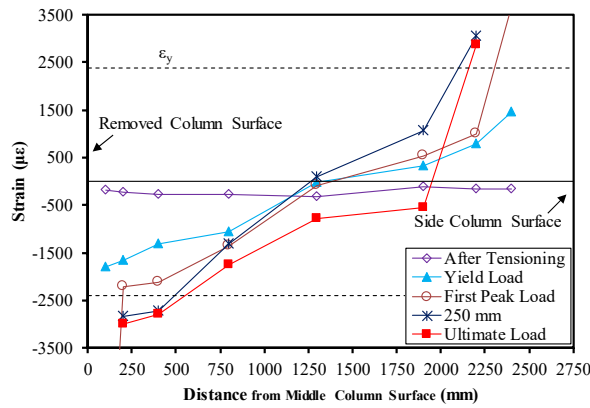
(d)



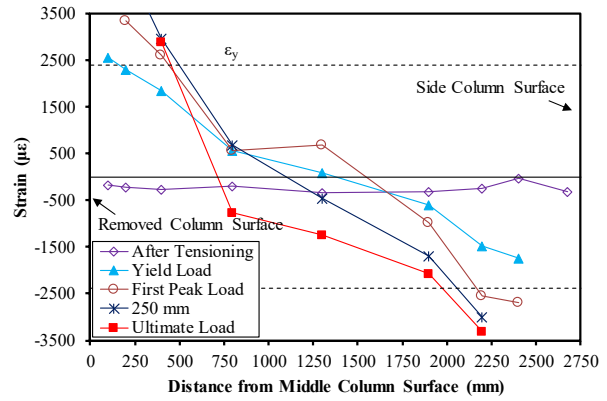
(a)



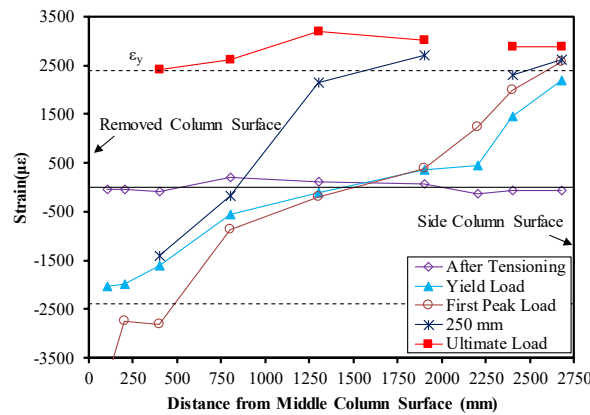
(b)



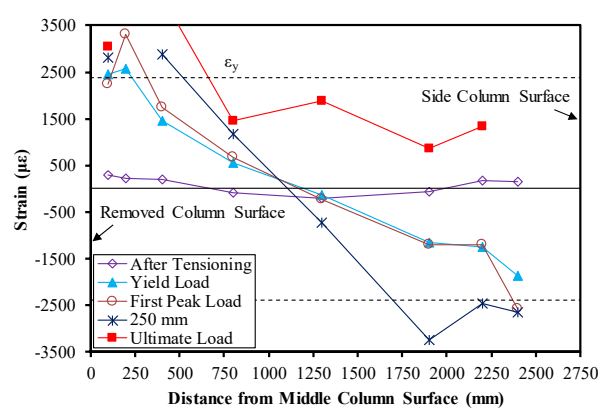
(c)



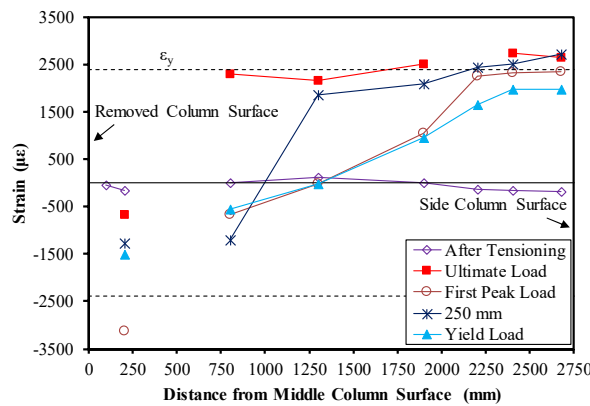
(d)



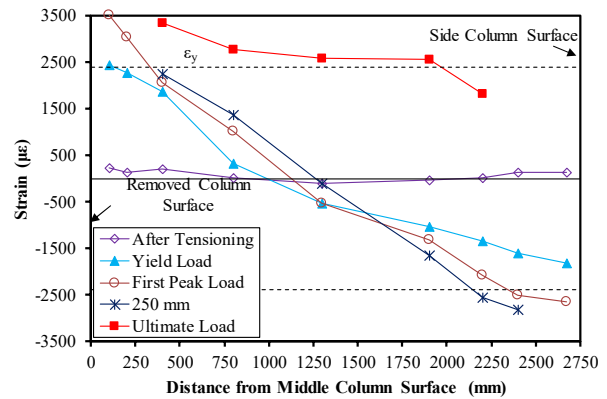
(e)



(f)



(g)



(h)

